

## Impact of Material Magnetization on the Magnetic Field Inside LCLS Cryomodule

A.C. Crawford and I. Terechkin

The problem of magnetic pollution became one of major issues during design stage of the LCLS-II cryomodule as the required quality factor of accelerating cavities exceeds  $10^{10}$ . Several studies were made in 2014 and 2015 to find possible configurations of global and local shielding [1], to propose and justify the use of compensating coils, and to analyze possible negative impact of magnetic devices located in the vicinity of the cavities [2]. As the desired configuration of the magnetic shielding in the cryomodule was implemented in the drawings, more subtle features started to emerge: certain parts used inside the cryomodule were found to have some (although relatively small) magnetization - permanent or induced. To understand possible impact of this magnetization, a study was made to set a framework for further investigation of the problem [3]. Although results of this study were on the optimistic side, claiming that the induced or permanent magnetization of the expected scale can be mitigated using existing magnetic shield system, certain details and features of the cryomodule and the shield still require obtaining quantitative information about the expected level of the field. Main of those details and features are the following:

- The presence of a tuning step motor, which was found to be magnetized;
- The structure of the tuning mechanism. It is made mostly of 316L alloy, but contains welded parts, which are found to be magnetic, and parts located or penetrating inside the magnetic shield.
- The support beams of the tuning mechanism. The beams made of 316L alloy protrude through the openings in the magnetic shielding; they found to be permanently magnetized to some extent.

The goal of this study is to understand to which extend the mentioned features can compromise the efficiency of the shielding.

### 316L stainless steel – relevant properties

316L alloy is fully austenitic (chromium-nickel stainless class) stainless steel containing 2%-3% molybdenum. Table below compares element content of the 316 and 316 L alloys. Alloy 310 also added to the table as it was found to be the best solution in previous studies (e.g. in [4]).

	Type 316 %	Type 316L %%	Type 310
Carbon	0.08 max.	0.03 max.	0.08 max.
Manganese	2.00 max.	2.00 max.	2.00 max.
Phosphorus	0.045 max.	0.045 max.	0.045 max.
Sulfur	0.030 max.	0.03 max.	0.03 max.
Silicon	0.75 max.	0.75 max.	0.75 max.
Chromium	16.00 - 18.00	16.00 - 18.00	24.00 - 26.00
Nickel	10.00 - 14.00	10.00 - 14.00	19.00 - 22.00
Molybdenum	2.00 - 3.00	2.00 - 3.00	0.75
Nitrogen	0.10 max.	0.10 max	-
Iron	Balance	Balance	Balance

Type 316L is an extra-low carbon version of Type 316 that minimizes harmful carbide precipitation due to welding. Free carbon content in the 316L alloy is less than 0.03%.

All austenitic stainless steels are generally non-magnetic with magnetic permeability just slightly exceeding 1.00. Permeability above 1.00 is associated with the amount of either ferritic or martensitic phase present in the austenitic steel; the excess of permeability depends on:

- cold working and heat treatment conditions;
- composition effects.

Due to low carbon content, 316L alloy is also less susceptible to sensitization than other austenitic steels. Sensitization occurs in the heat-affected zone where a peak temperature of about 900 to 1600 F (482 to 871 C) is reached. Chromium carbides precipitate on grain boundaries, and in the process of doing so, chromium as an alloy element is depleted in the metal adjacent to the grain boundaries.

The microstructure of austenitic stainless steel can also be changed by a process called **martensitic stress induced transformation** (MSIT). This is a microstructural change from austenite to martensite and the transformation can occur due to **cold working** (the process by which many fasteners are made) as well as **slow cooling** from austenitizing temperatures. After cold working or slow cooling an austenitic stainless steel will have an appreciable level of martensitic microstructure. Due to martensite being magnetic, the once nonmagnetic austenitic stainless steel will now have a degree of magnetism. The degree to which this occurs depends on the compositional effects of austenite stabilizing elements. High nickel or nitrogen bearing grades tolerate more cold working before localized increases in permeability are noticed.

During the welding of this steel, the following structural changes can also occur:

- Some of the austenite in the parent material can transform to delta ferrite at high temperatures and on cooling this is partly retained at room temperature.
- Welding filler rods and wires are usually 'over-alloyed' to prevent dilution in the fusion zone but more importantly are balanced to have deliberately high ferrite levels of 5% or sometimes 10%, to minimize the risk of hot cracking during welding.

The increase in permeability due to any of processes described above can be reversed by full solution annealing at temperatures around 1050 / 1120 °C with rapid cooling. This transforms any cold-formed martensite back to austenite, the non-magnetic phase.

In [4], permeability of several austenitic steels was measured on the samples in the “as received” condition and after annealing, electro-polishing, welding using different welding alloys, and post-weld annealing. The goal of the study was to find an alloy that would keep a low (less than 1.02) permeability after welding without additional annealing. The best results were found when 310 alloy was used, but using proper weld rod with 316L alloy also resulted in the acceptable output.

Another relevant study was made in [5], where several types of stainless steel are compared to find an optimal chemistry for use in superconducting accelerator magnets.

**Calculation of magnetic field of magnetized bodies.**

First, let's specify the approach that will be used to calculate the field resulted from the magnetization: induced or permanent.

In the case of **induced magnetization**, the added field is defined by the material's magnetic susceptibility, so the following definition of the flux density will be used:

$$B_i = \mu_0 H_i + M \rightarrow \mu_0 H_i + \mu_0 \xi H_i = \mu_0 \mu_r H_i$$

where  $\xi$  is magnetic susceptibility. For ellipsoids, in accordance with [3], expressions for the magnetic field measured in the direction of the long axis Z is:

$$H_z = 2m/(4\pi\mu_0 z^3)$$

As the magnetic moment m is the integral of the magnetization over the volume:  $m = \int M dV$ , for the ellipsoids (with uniform magnetic field inside)

$$m = M \cdot V$$

By definition,

$$M = \mu_0(\mu_r - 1)H_i$$

The magnetic field  $H_i$  inside rotation ellipsoid can be calculated using the following expression:

$$H_i = H_0/[1+N \cdot (\mu_r - 1)]$$

where N is the demagnetization factor that can be found using the next formula:

$$N = 1/(p^2-1) \cdot \{p/\sqrt{(p^2-1)} \cdot \ln[p+\sqrt{(p^2-1)}]-1\}$$

with the ellipsoid form factor

$$p = a/b.$$

Using expression for the field  $H_i$  we can re-write expression for the induced magnetization:

$$M = \mu_0(\mu_r - 1)H_0/[1+N \cdot (\mu_r - 1)]$$

Similarly, the magnetic dipole moment

$$m = V \cdot \mu_0 H_0 (\mu_r - 1) / [1+N \cdot (\mu_r - 1)]$$

If  $\xi = \mu_r - 1 \ll 1$ , the magnetic moment  $m \approx B_0 V \cdot (\mu_r - 1)$  is relatively small. If  $N \cdot (\mu_r - 1) \gg 1$ , magnetization  $M \approx B_0/N$  and  $m \approx B_0 V/N$ . As N is always less than 1, often significantly, the dipole magnetic momentum can be highly intensified in the material with high permeability. In this case, the magnetization of an ellipsoid does not depend on the permeability. It reaches its maximum that depends on a particular form factor p. E.g. for  $p = 5$ ,  $N = 0.056$ ,  $V = 5 \text{ cm}^3$ , and  $B_0 = 1 \text{ G}$ , magnetization  $M \approx 17.9 \text{ G}$  and  $m \approx 9 \cdot 10^{-9} \text{ T} \cdot \text{m}^3$ . With this magnetization and volume of the material, the additional field outside the magnetized body at the distance 5 cm from the center of the magnetic dipole moment  $B = m/2\pi z^3 \approx 0.1 \text{ G}$ . At 10 cm, it is  $\sim 12 \text{ mG}$ . It worth to stress here that higher values of permeability cannot make the induced magnetization more than  $1/N$  times higher than the applied field.

If the volume of an ellipsoid is fixed at  $1 \text{ cm}^3$  and different shapes are used, the maximum values of magnetizations in the background field of 1 G are shown in Table 1 depending of the form factor p:

Table 1. Limits of induced magnetization for different form factors

p	1.1	2	5	10	20
M (G)	3.25	5.76	17.9	49.3	148

These values can be treated as the values of the magnetic dipole moment  $m$  per  $1 \text{ cm}^3$  unit of volume and can be taken as the ultimate limits of residual magnetizations of the material after it

was exposed to a 1 G environment field. The numbers scale linearly with the field, so if there is a chance of exposure to a 10 G field, corresponding increase of the magnetization must be taken into account.

In the case of the **permanent magnetization**, in the absence of the environmental field, we also need to take into account both the shape of the magnetized body and the permeability of the material. As the remnant flux density is a material constant, the higher the permeability is, the lower inner magnetic field is, and hence the lower field is expected in the surrounding space (in accordance with the Ampere’s law).

Tables below present results of calculation of the magnetic field inside a magnetized ellipsoid and at the distance 50 mm from the center for different values of permeability. Remnant flux density  $B_r = 1$  kG is assumed and two values of the form factor are used:  $p = 2$  and  $p = 5$ .

Table 2. Impact of remnant magnetization of ellipsoids depending on permeability;  $p = 2$

mu	1	10	100	1000	10000
$B_{in}$ (G)	826.3	322.6	45.45	4.74	0.476
$H_{in}$ (Oe)	-173.5	-67.75	-9.55	-0.995	-0.1
$K = H_{in}/B_{in}$	-0.21	-0.21	-0.21	-0.21	-0.21
$B_{50mm}$ (G)	0.0097	0.0038	$5.3 \cdot 10^{-4}$	$5.6 \cdot 10^{-5}$	$5.6 \cdot 10^{-6}$

Table 3. Impact of remnant magnetization of ellipsoids depending on permeability;  $p = 5$

mu	1	10	100	1000	10000
$B_{in}$ (G)	944	630	145	16.6	1.7
$H_{in}$ (Oe)	-56	-37	-8.55	-0.987	-0.1
$K = H_{in}/B_{in}$	-0.059	-0.059	-0.059	-0.059	-0.059
$B_{50mm}$ (G)	$2.45 \cdot 10^{-2}$	$1.63 \cdot 10^{-2}$	$3.8 \cdot 10^{-3}$	$4.4 \cdot 10^{-4}$	$4.4 \cdot 10^{-5}$

Coefficient K in the table is defined as  $K = H_{in}/B_{in}$ . In both tables the values of K are constant and quite close to corresponding demagnetization factors N (0.19 for  $p = 2$  and 0.056 for  $p = 5$ ). Basically this coefficient is a tangent of the load curve for a permanent magnet, so it shows effective demagnetizing by the gap (which is the surrounding space).

As one would expect, if to take the ratio  $(B_{in} - B_r)/H_{in}$ , it coincides with the assumed permeability.

The residual field (and hence the magnetization) inside the ellipsoid can be expressed using a simple relationship that works well at high permeability (e.g.  $\mu_r > 10$ ):

$$B_{in} = B_r / (1 + N\mu_r) .$$

Analysis of the results summarized by the tables above shows that the worst case for the purpose of our study is having a residual magnetization in a material with low permeability. So the next question is what this remnant flux density could be.

**Remnant flux density in the material**

Permeability measurements on samples made of 316L alloy with or without welded seams and no annealing made routinely results in the values of permeability  $\mu_{eff} > 1$  [7]. According to what was found earlier, this permeability is due to the presence of the martensitic phase.

Magnetization of this phase can be taken into account by using the magnetic susceptibility  $\xi_{\text{mart}}$  and the residual flux density  $B_{r_{\text{mart}}}$ ; the next expression can be used to evaluate the amount of the martensitic phase in the volume of the material:

$$\xi_{\text{eff}} = \xi_{\text{mart}} \cdot V_{\text{mart}} / V_{\text{tot}}$$

Knowing  $\xi_{\text{mart}}$  and measuring  $\xi_{\text{eff}}$  we can find the relative volume of the martensitic phase. From here expected residual flux density in the material can be evaluated:

$$B_{r_{\text{eff}}} = B_{r_{\text{mart}}} \cdot V_{\text{mart}} / V_{\text{tot}}$$

For example, assuming the residual magnetization of the martensitic phase of  $\sim 5000$  G, permeability  $\mu_{\text{mart}} = 200$ , and the measured effective permeability of  $\sim 1.1$  ( $\xi_{\text{eff}} = 0.1$ ), we get

$$B_{r_{\text{eff}}} = 2.5 \text{ G.}$$

This is the maximum field level we can measure near the end of an elliptical sample of the material. So, the modeling of the field generated by the piece made of this material must use the magnetization  $M = 2.5$  G and permeability  $\mu \approx 1$ .

### Geometry

Because subtle details of the chosen design must be analyzed, a 3D magnetic field needs to be applied to the studied structure and a 3D model geometry is needed. On the other hand, only one cavity with two-layer shielding ( $\mu = 9000$ ) can be used inside the cryomodule to get trustable results. Low-carbon steel magnetic properties were assigned to the walls of the vacuum vessel, the compensation coils (as in [1]) were employed, and next values of the environmental magnetic field components were used:

- $H_X = 0.15$  Oe (longitudinal, along the axis),
- $H_Y = 0.25$  Oe (transverse horizontal),
- $H_Z = 0.5$  Oe (transverse vertical)

Fig. 1 shows the geometry accepted for the modeling.

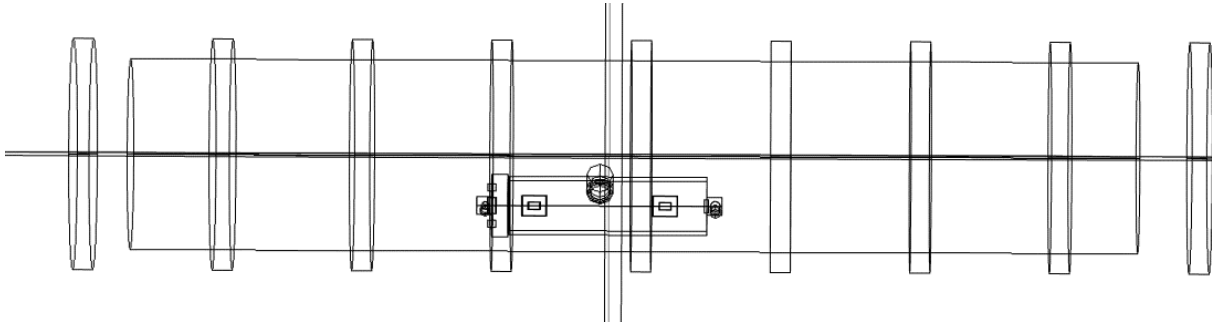


Fig. 1. Cryomodule with the compensation coils and with the dressed and shielded RF cavity.

Horizontal axis in the Fig. 1 is X; it is centered in the middle of the cavity. The left border of the primary magnetic shield is at  $X = -535$  mm; the right border of this shield is at  $X = 532$  mm. In the first (left) cell of the cavity inside the magnetic shield, the maximum cell radius corresponds to the coordinate  $X = -455$  mm.

All openings in the shield studied in [1] are respected.

**Base Magnetic Field**

As a result of the study in [1], the distribution of the magnetic field inside the local magnetic shielding (in the area where the cavity is located) was found, which is replicated in figures 2, 3, 4, and 5.

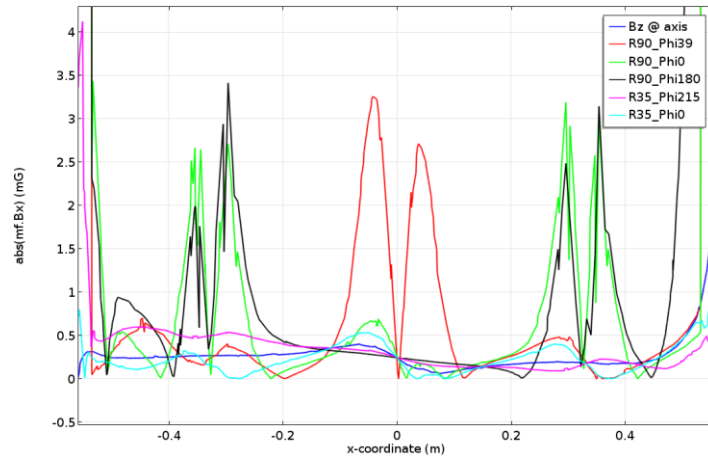


Fig. 2. X component of magnetic field along several lines parallel to the axis of the cavity.

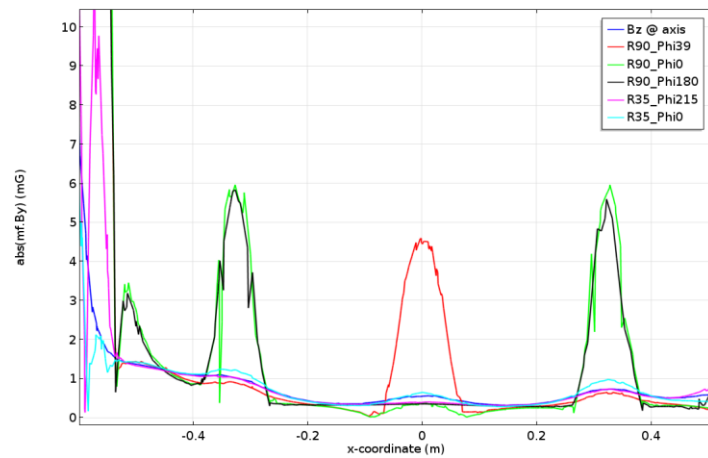


Fig. 3. Y component of magnetic field along several lines parallel to the axis of the cavity.

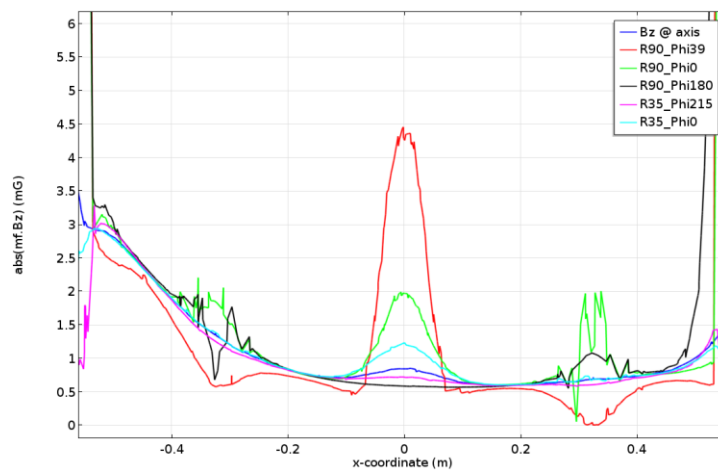


Fig. 4. Z component of magnetic field along several lines parallel to the axis of the cavity.

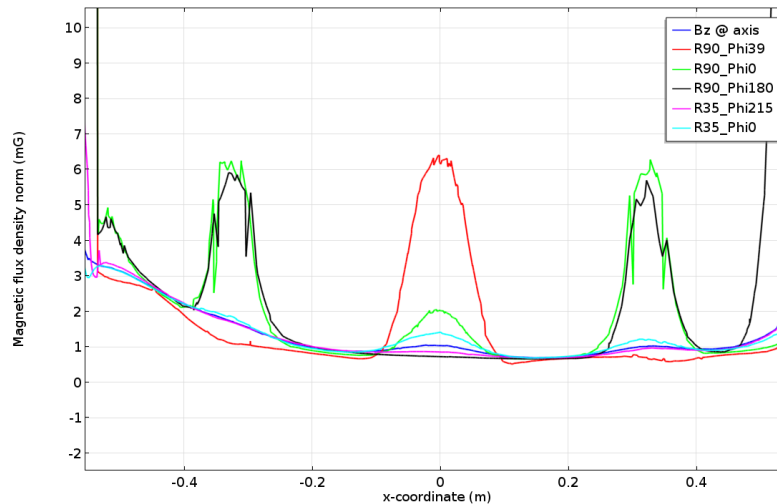


Fig. 5. Absolute value of magnetic field along several lines parallel to the axis of the cavity.

The magnetic field inside the shield is below 6 mG; the input for the total magnetic field comes from all the components. That's why it is important to make 3D modeling in this case. Graphs in figures 2 through 5 will serve as a reference for further study, where we will add, one by one, features suspected to be magnetic field pollutants.

### Step motor impact

The most prominent part installed near the cavity and long suspected in being strongly magnetized is a step motor. In 2014, a study was made by D. Sergatskov [6] to quantify the magnetization of the motor (VSS322.200.1.2 GPL UHVC). It was found that the magnetic field around the motor fits the field of a dipole with the magnetic moment  $\mathbf{m} = 2.5 \cdot 10^{-7} \text{ T} \cdot \text{m}^2$  directed along the longitudinal axis of the motor. This value of the magnetic moment was used to design local shield to protect cavities tested in the vertical test stand and not equipped with local shielding. Since that time, the size of the motor was increased, and VSS52 series was accepted in a baseline design. Paradoxically, the measured dipole momentum of this motor [6] appeared less strong:  $\mathbf{m} = 1.0 \cdot 10^{-7} \text{ T} \cdot \text{m}^2$ . Most plausible explanation of the mere existence of this momentum is that there exists some uncompensated part of the radial magnetization of the permanent magnets in the motor, or the shaft of the motor, which is made of magnetically hard steel, has acquired some magnetization. Both ways imply some statistic uncertainty. The position of the effective dipole momentum was also found in [6] as located  $\sim 106 \text{ mm}$  from the shaft side of the motor or  $\sim 25 \text{ mm}$  from the connector side.

As no statistical studies exist on the subject, for further study, we will use the value of dipole momentum that is twice as strong as in the measured VSS32 motor, that is  $\mathbf{m} = 5 \cdot 10^{-7} \text{ T} \cdot \text{m}^2$ . In accordance with [3], this momentum can be introduced as a magnetized cylinder with 10 mm radius, 20 mm long, made from the material with the unit permeability, and with the residual magnetization of  $\sim 0.08 \text{ T}$ .

As the position of the motor is strictly defined by the design (192 mm transverse shift in the horizontal plane, 55 mm shift in the vertical plane, and 164 mm from the plane of the cavity's

first cell maximum radius), the magnetic modeling is straightforward. A graph of the absolute value of the field distribution is shown in Fig. 6.

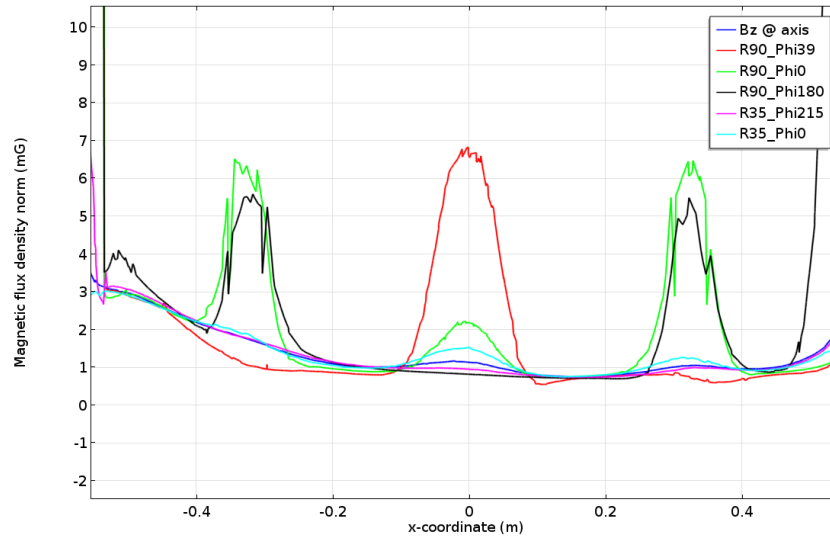


Fig. 6. Absolute value of the magnetic field in the presence of a magnetized step motor.

Very modest redistribution of the magnetic field in the area occupied by the first cell is an indicator that there is no need for additional local devoted magnetic shield around the motor.

**Impact of welding**

In accordance with what is known about magnetization problems associated with the welding made on 316L steel, there should be no problems if the demagnetization process is made correctly. The steel should become fully austenitic and non-magnetic. Nevertheless, let’s evaluate possible outcome if the demagnetization procedure did not work as desired. Effective permeability measured at the ends of the welded seams was measured to be ~1.1 [7]. According to what was found earlier in this note, the magnetization level inside the welded seam is ~2.5 G.

Let’s make an assumption about the volume of the material affected during welding. With the weld depth of ~4 mm, let’s assume that the affected area, that is the area where the temperature exceeds ~1150°C, is ~100 mm<sup>2</sup> in cross-section and 50 mm long. The slow cooling after welding is the process that helps in the transformation from the austenitic phase to the martensitic one. Then the magnetic moment

$$m = M \cdot V = 2.5 \cdot 10^{-4} \text{ T} \times 5 \cdot 10^{-6} \text{ m}^3 = 1.25 \cdot 10^{-9} \text{ T} \cdot \text{m}^2$$

This is much smaller than what was measured for the step motor. Modeling made similar to what was made for the impact of the motor that included two seams in the Z direction and two seams in the X direction showed that impact of the welded seams can be neglected.

**Magnetized ball if the bearings located outside the magnetic shield**

Using the same approach, the field generated by **steel bearings** can be evaluated. In this case both the permeability and the residual flux density are high. In the case of ball bearings, the form factor is  $p = 1$  and  $N = 1/3$ . Assuming  $B_r = 5000 \text{ G}$  and  $H_c = 1 \text{ Oe}$ , we have effective permeability in the demagnetizing part of the magnetization curve of 5000. At a result, if the balls were fully magnetized, we can expect residual magnetic field inside the balls

$B_{in} = B_r / (1 + N\mu_r) = 5000 / (1 + 1/3 \cdot 5000) \approx 3 \text{ G}$ . Even assuming the radius of the balls in the bearings of  $\sim 5 \text{ mm}$ , this results in the magnetic moment of one ball  $m \approx 1.5 \cdot 10^{-10} \text{ T} \cdot \text{m}^3$ .

It is  $\sim 10$  times less than in the case of welded seam. Even 100 balls magnetized in the same direction will not provide dangerous levels of magnetic field inside the shield.

**Impact of the tuning block support bars.**

Support bars are made of stainless steel and penetrate through the holes in the magnetic shield in the vicinity of the first cell of the cavity (Fig. 7).

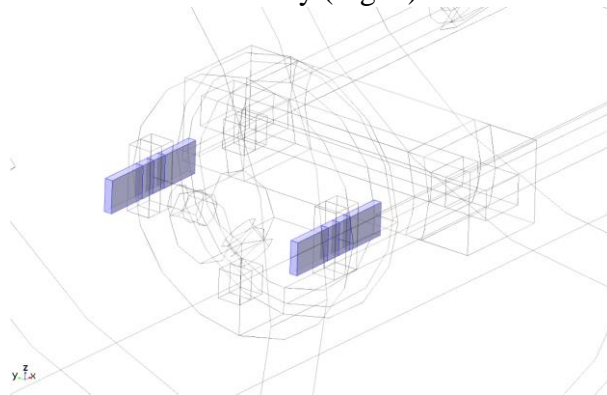


Fig. 7. Support bars.

If magnetized, the support bars present clear danger by exposing the first cell to the associated magnetic field. According to [7], the maximum field level at the end of the parts is below 0.5 G. Having in mind the shape of the bars, the maximum flux density inside the bars of  $\sim 1 \text{ G}$  can be expected. Also this level of the residual field allows making evaluation of the relative volume of the martensitic phase:

$$V_{mart} / V_{tot} = M_{eff} / M_{mart} = 1 / 5000 = 2 \cdot 10^{-4}.$$

This makes the expected permeability of the bars  $\mu_{eff} \approx 1.04$ .

Even using  $\mu_{eff} \approx 2$  does not result in any significant excess of the field in the area of the cavity's first cell. Fig. 8 below shows the accumulated field environment in the presence of the step motors and the support bars; it must be compared with Fig. 5.

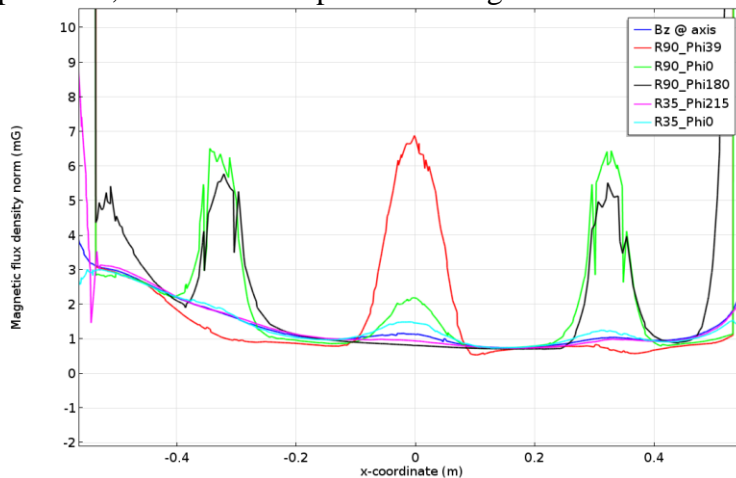


Fig. 8. Absolute value of the magnetic field in the presence of a magnetized step motor and support bars (assumed  $\mu_{eff} = 2$ )

Let's assume that the bars have 1 G residual magnetization. Graph in Fig. 9 shows the field due to all assumed disturbances.

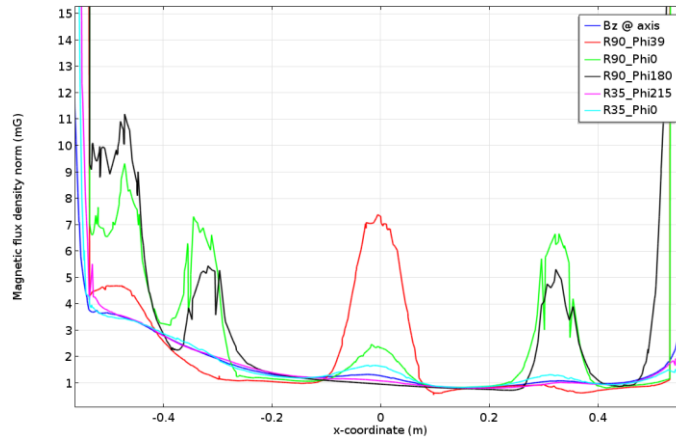


Fig. 9. Absolute value of the magnetic field with support bars magnetized to 1 G.

The magnetization of the bars does modify the field distribution, but does not make it **much** worse. Both X and Y component are affected by the bars as one can see in Fig. 10 and Fig. 11.

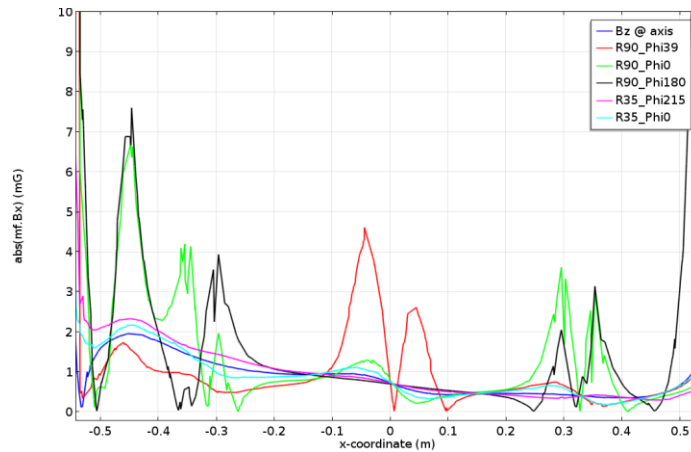


Fig. 10. X component of the magnetic field with support bars magnetized to 1 G.

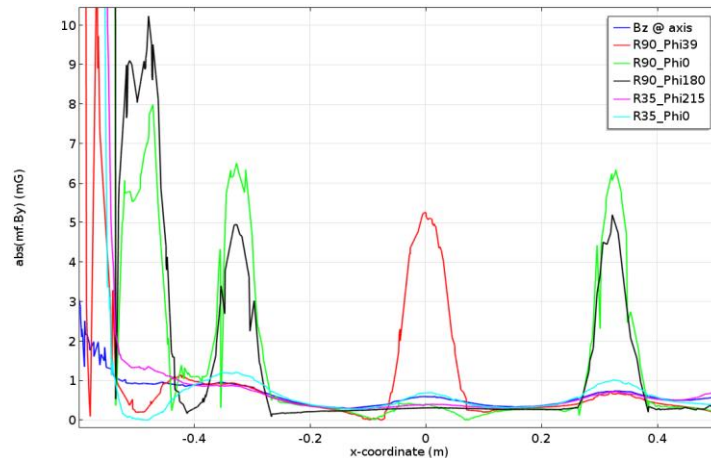


Fig. 11. Y component of the magnetic field with support bars magnetized to 1 G.

Field map in Fig. 12 shows magnetic flux density distribution in the center plane of the cavity for the first three cells. Saturated red color covers the area with the field >10 mG.

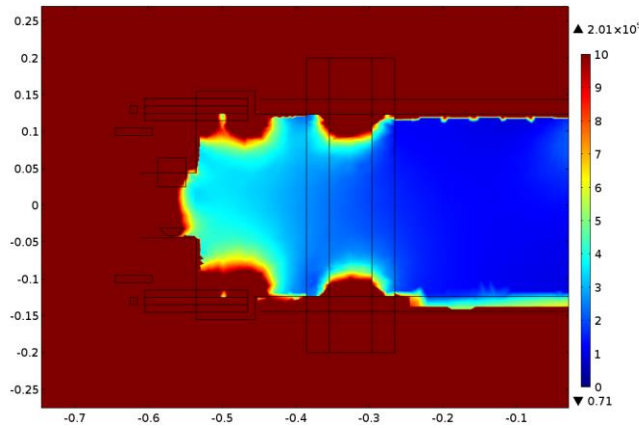


Fig. 12. Field map in the horizontal plane.

**Impact of the magnetized balls of the fast tuner safety guards.**

Another features that can bring undesired magnetic field inside the magnetic shielding are two balls that are used to transfer force from the fast tuner to the cavity through the safety rods. They are made of Wolfram Carbide and demonstrate significant magnetization due to some presence of Cobalt. Magnetic measurements made around the balls show that the residual magnetization can reach ~ 10 G [7]. As the balls are inside the magnetic shield, simple evaluation, like made in [3] can be used to find the expected field level in the cavity area. It shows possible increase of the field to the level in excess of the allowed 10 mG.

To take into account existing shielding, full modeling was made. Two balls, each 7 mm in diameter, magnetized to 10 Gauss, were placed inside the shield at the distance 61 mm from the plane of the maximum radius of the first cell (X = -515 mm). The distance of the balls from the axis was 84.5 mm, so they were near the penetration windows made in the first layer of the shield for the safety rods. Fig. 13 compares magnetic field maps in the vertical plane (through the balls) for the cases of zero and 10 G magnetization; no magnetized support bars were used in this case.

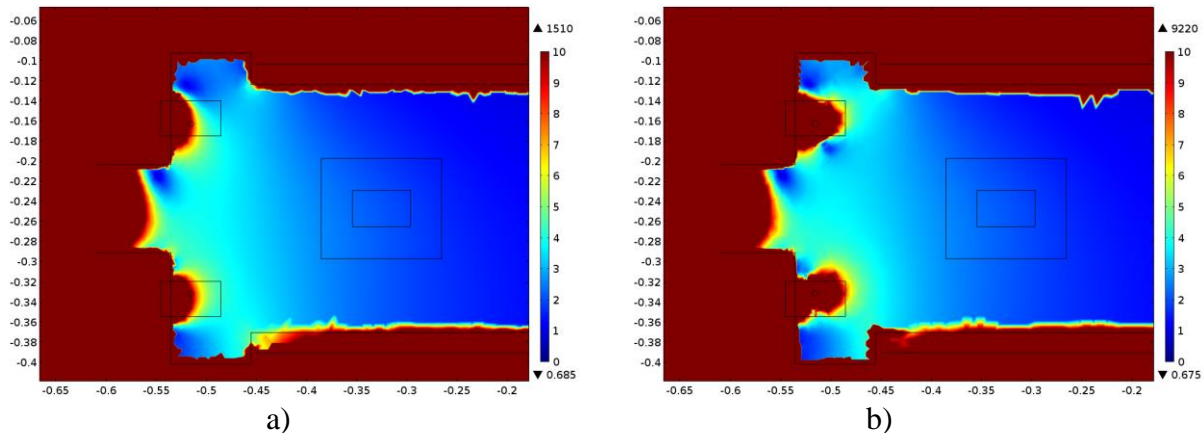


Fig. 13. Field map in the vertical plane without (a) and with (b) magnetized balls.

One can see that the 10 mG boundary (red color background) becomes much closer to the area where the 1-st cell of the cavity is when the magnetization is made on. Magnetic field at the point  $X = -490$  mm (35 mm from the cavity's maximum R position  $X = -455$  mm) is  $\sim 5$  mG. At  $X = -495$  mm (40 mm from the cavity's maximum R position), the field reaches the 10 mG level.

#### Impact of the rods of the fast tuner safety guards.

Besides the magnetized Wolfram-Carbide balls that are located inside the magnetic shield there are also safety guard rods that also penetrate the shield through the two openings in the shield. The rods are made of 316L steel, so, in accordance with what was found earlier, even if the rods are not annealed, we should not expect residual magnetization much higher than  $\sim 1$ G. Nevertheless, the size of the rods and their proximity to the cavity forces to check on possible field on the cavity surface due to this magnetization.

The rods are 185 mm in length and 8 mm in diameter. They penetrate inside the shield through the rectangular openings in the shield. The axis of each rod is  $\sim 100$  mm from the axis of the cavity, and location of each rod's end inside the shield is  $\sim 40$  mm from the plane of the maximum cavity radius, which is quite close to the cavity's surface.

The field map in the presence of the magnetized rods is shown in Fig. 14. It must be compared with the map in Fig. 13-b for the magnetized ball.

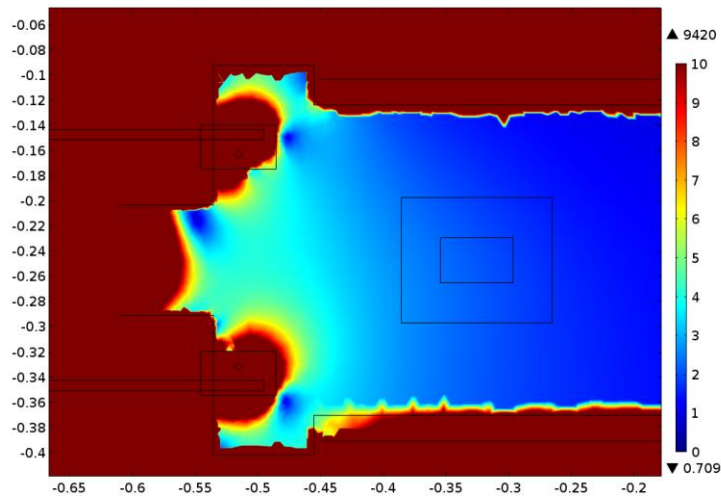


Fig. 14. Field map in the vertical plane with magnetized safety rods.

One can see visible expansion of the zone with  $B > 10$  mG, which moves  $\sim 1$  mm closer to the cavity's surface. So, as in the case with the magnetized balls, the rods penetrating through the openings further increase undesired magnetic field. The rods must be annealed to restore fully austenitic state of the material, or be made of a non-magnetic material.

**Conclusion.**

As a result of this study, the following statements can be made:

- Design of the protective magnetic shielding provides adequate protection against induced or permanent magnetization of the parts installed in the vicinity of the cavity outside the shielding. This includes the step motor, which does not need additional local protective magnetic shield.
- The strong effect is expected from the support bars that penetrate the shield through technological openings. To avoid problems, it is recommended to anneal the bars using proper annealing procedure or to use fully non-magnetic material.
- Undesirable increase of magnetic field is expected when Wolfram-Carbide balls are used inside the magnetic shielding. Replacing the material of the balls by a fully non-magnetic one would help to reduce the field on the cavity surface.
- Additional increase of magnetic field is due to the presence of the safety rods made of 316L steel, if the rods are not annealed. Using non-magnetic material instead will resolve the problem.

**References:**

1. I. Terechkine, "Some Options for Improving the Effectiveness of Magnetic Shielding in the LCLS-II Cryomodule", FNAL TD note TD-14-006, November 2014.
2. I. Terechkine, "Fringe Field of a Focusing Quadrupole in the Beam Line of the LCLS Cryomodule", FNAL TD note TD-14-005, November 2014.
3. I. Terechkine, "Magnetic Field of Magnetized Ellipsoids", FNAL TD note TD-15-006, June 2015
4. N. Wilson and P. Bunch, "Magnetic Permeability of Stainless Steel for use in Accelerator Beam Transport Systems", PAC 1991, transactions, pp. 2322 – 2324.
5. D. Larbalestier, "Selection of Stainless Steel for the Fermilab Energy Doubler/Saver Magnets", FNAL, TM-745, Oct. 1977.
6. D. Sergatskov, private communication.
7. A.C. Crawford, private communication.